ATLAS NOTE

ATLAS-CONF-2011-060

April 12, 2011

Measurement of the production cross section for W-bosons in association with jets in pp collisions using 33 pb^{-1} of data at $\sqrt{s}$ = 7 TeV with the ATLAS detector

The ATLAS Collaboration

Abstract

This note reports the measurement of the inclusive W+jets cross section in proton-proton collisions at a centre-of-mass energy of 7 TeV at the LHC, with the ATLAS detector. Cross sections, in both the electron and muon decay modes of the W boson, are presented as a function of jet multiplicity. Differential cross sections are measured with respect to transverse momenta, p_{T}, of jets for events with jet multiplicities $N_{\mathrm{jet}} = 1{-}4$. The differential cross sections as a function of H_{T}, defined as the sum in p_{T} of the jets, lepton and neutrino, for $\geq 1{-}4$ jet events are also shown. Measurements are presented of the ratio of cross sections $\sigma(W+ \geq N_{\mathrm{jet}})/\sigma(W+ \geq N_{\mathrm{jet}} - 1)$ for inclusive jet multiplicities $N_{\mathrm{jet}} = 1{-}5$. This note, expanding upon an earlier measurement with the ATLAS detector, is based on an integrated luminosity of 33 pb^{-1} and includes improved jet energy scale and luminosity uncertainties. The results have been corrected for all known detector effects and are quoted in a limited and well-defined range of jet and lepton kinematics. The measured cross sections are compared to particle level predictions based on perturbative QCD. Next-to-leading order calculations from MCFM, studied here for $N_{\mathrm{jet}} \leq 2$, and BLACKHAT-SHERPA, studied here for $N_{\mathrm{jet}} \leq 3$, are found in good agreement with the data. Leading-order multiparton event generators, normalized to the NNLO total cross section, describe the data well for all measured jet multiplicities.

1 Introduction

The study of massive vector boson (V, where $V = W$ or Z) production in association with one or more jets (V+jets) is an important test of quantum chromodynamics (QCD). In addition, V+jets processes are a significant background to studies of Standard Model processes such as $t\bar{t}$ or single-top production, as well as searches for the Higgs boson and for physics beyond the Standard Model. Measurements of the cross section and kinematic properties of V+jets processes and comparisons to theoretical predictions are therefore of significant interest. This note reports on a measurement at the Large Hadron Collider (LHC) of the W+jets cross section in proton-proton (pp) collisions at a centre-of-mass energy ($\sqrt{s}$) of 7 TeV, in both electron and muon decay modes of the W-boson, with the ATLAS detector. The measurement is based on an integrated luminosity of approximately 33 pb^{-1} and is an extension of an earlier ATLAS measurement with 1.3 pb^{-1} [1].

The cross section measurements are presented as a function of jet multiplicity and of the transverse momentum (p_{T}) of each jet (up to the fourth jet) in each event. Measurements are also presented of the ratio of cross sections $\sigma(W+ \geq N_{\mathrm{jet}})/\sigma(W+ \geq N_{\mathrm{jet}} - 1)$ for inclusive jet multiplicities $N_{\mathrm{jet}} = 1{-}5$. The differential cross sections as a function of H_{T} where H_{T} is the scalar sum of the p_{T} of jets passing the selection, the lepton p_{T} and the missing transverse energy for $\geq 1{-}4$ jet events are also shown. The results have been corrected for all known detector effects and are quoted in a limited and well-defined range of jet and lepton kinematics, fully covered by the detector acceptance, so as to avoid model-dependent extrapolations and to facilitate comparisons with theoretical predictions. In addition to the ATLAS results [1], measurements of W+jets production in proton-antiproton collisions at $\sqrt{s} = 1.96$ TeV were published by the CDF Collaboration [2] and have been presented by the CMS Collaboration for proton-proton collisions at $\sqrt{s} = 7$ TeV [3]. Theoretical calculations at next-to-leading-order (NLO) in perturbative QCD (pQCD) have been computed for up to four jets for W production [4, 5]. For this note, only comparisons with NLO pQCD calculations for $N_{\mathrm{jet}} \leq 3$ were available; higher jet multiplicities are compared only to leading-order (LO) calculations.

2 The ATLAS Detector

The ATLAS detector [6, 7] consists of an inner tracking system (inner detector, or ID) surrounded by a thin superconducting solenoid providing a 2T magnetic field, electromagnetic and hadronic calorimeters and a muon spectrometer (MS). The ID consists of pixel and silicon microstrip (SCT) detectors, surrounded by the transition radiation tracker (TRT). The electromagnetic calorimeter is a lead liquid-argon (LAr) detector, split into barrel ($|\eta| < 1.475$) and endcap ($1.375 < |\eta| < 3.2$) regions. Hadron calorimetry is based on two different detector technologies. The barrel ($|\eta| < 0.8$) and extended barrel ($0.8 < |\eta| < 1.7$) calorimeters are composed of scintillator/steel; the hadronic endcap calorimeter ($1.5 < |\eta| < 3.2$) are LAr/Cu. The forward calorimeters ($3.1 < |\eta| < 4.9$) are instrumented with LAr/Cu and LAr/W that provide electromagnetic and hadronic energy measurements, respectively. The MS is based on three large superconducting toroids arranged with an eight-fold azimuthal coil symmetry around the calorimeters, and a system of three stations of chambers for the trigger and for precise measurements. The nominal pp interaction point at the centre of the detector is defined as the origin of a right-handed coordinate system. The positive x-axis is defined by the direction from the interaction point to the centre of the LHC ring, with the positive y-axis pointing upwards, while the beam direction defines the z-axis. The azimuthal angle ϕ is measured around the beam axis and the polar angle θ is the angle from the z-axis. The pseudorapidity is defined as $\eta = -\ln\tan(\theta/2)$ and rapidity is defined as $y = 0.5{\times}\ln[(E+p_z)/(E-p_z)]$.

3 Simulated Event Samples

Simulated event samples were used for most of the background estimates, for the correction of the signal yield for detector effects and for comparisons of the results to theoretical expectations. The detector simulation [8] was performed using GEANT4 [9]. The simulated event samples are summarised in Table 1 for signal simulations and Table 2 for the background simulations. The ALPGEN and MC@NLO samples were interfaced to HERWIG for parton shower and fragmentation processes and to JIMMY v4.31 [10] for underlying event simulation. Parton density functions (PDF) were: CTEQ6L1 [11] for the ALPGEN and SHERPA samples, MRST 2007 LO* [12] for PYTHIA, MSTW2008 [13] for FEWZ [14] and CTEQ6.6M [15] for MC@NLO. For the diboson samples, the PDF set was MRST 2007 LO* and JIMMY was used for the underlying event simulation. For the POWHEG samples, the PDF set was CTEQ6.6M for the NLO matrix element calculations, while CTEQ6L1 was used for the parton showering and underlying event via the POWHEG interface to PYTHIA. The radiation of photons from charged leptons was treated in HERWIG and PYTHIA using PHOTOS v2.15.4 [16]. TAUOLA v1.0.2 [17] was used for tau decays. The underlying event tune was the ATLAS MC09 tune [18] for the ALPGEN samples, PYTHIA inclusive vector boson production, and PYTHIA QCD samples. The POWHEG sample used the ATLAS MC09 tune with one parameter adjusted.[1] The AMBT1 [19] tune was used to describe the underlying event in the PYTHIA W+jets samples. The samples generated with SHERPA used the default underlying event tune determined from lower energy measurements and extrapolated to the LHC energies. Samples were generated with minimum bias interactions overlaid on top of the hard-scattering event in order to account for the multiple pp interactions in the same beam crossing (pile-up) experienced in the data. These samples were then reweighted such that the distribution of the number of primary vertices matched that of the data.

Physics process	Generator	Scale factor
$W \to \ell\nu$ inclusive ($\ell = e, \mu, \tau$)	PYTHIA 6.4.21 [20]	1.17
$W \to \ell\nu$ + jets ($\ell = e, \mu$, $0 \leq N_{parton} \leq 5$)	ALPGEN 2.13 [21]	1.21
$W \to \ell\nu$ + jets ($\ell = e, \mu$, $0 \leq N_{parton} \leq 4$)	SHERPA 1.1.3 [22]	1.19
$W \to \ell\nu$ + jets ($\ell = e, \mu$)	PYTHIA 6.4.21 [20]	—
$W \to \ell\nu$ + jets ($\ell = e, \mu$)	MC@NLO 3.3.1 [23]	—

Table 1: Signal simulated event samples used in this analysis. The predicted W inclusive cross section is 10.46 nb [14] at next-to-next-to-leading-order (NNLO). The W samples are normalised to the inclusive cross sections and the resulting scale factors are also shown. For PYTHIA, the inclusive W sample is based on a $2 \to 1$ matrix element merged with a $2 \to 2$ matrix element and a leading-logarithmic parton shower; the W+jets samples are based on $2 \to 2$ matrix elements. The scale factors for the PYTHIA W+jets and MC@NLO simulations are not shown since these samples are only used for the non-perturbative corrections and the quark/gluon jet energy scale uncertainty, respectively. Details of PDF sets, final-state photon radiation, and underlying event tunes are given in the text.

4 Data and Event Selection

The data used in this analysis were collected during the LHC 2010 run. Application of beam, detector, and data-quality requirements resulted in a total integrated luminosity of 33 pb^{-1}. The uncertainty on

[1] The cutoff for multiple parton interactions, PARP(82), was adjusted from 2.3 to 2.1 GeV, suitable for the CTEQ6L1 PDF.

Physics process	Generator	$\sigma \cdot$ BR (nb)		
$Z \to \ell\ell$ + jets ($m_{\ell\ell} > 40$ GeV, $0 \leq N_{parton} \leq 5$)	ALPGEN 2.13 [21]	1.07	NNLO	[14]
$Z \to \tau\tau$ ($m_{\ell\ell} > 60$ GeV)	PYTHIA 6.4.21 [20]	0.85	NNLO	[14]
$t\bar{t}$	POWHEG-HVQ			
	v1.01 patch 4 [24]	0.16	NLO+NNLL	[25]
Single-top $t \to \ell\nu q$ (s-channel)	MC@NLO 3.3.1 [23]	4.3×10^{-4}	NLO	[26]
Single-top $t \to \ell\nu q$ (t-channel)	MC@NLO 3.3.1 [23]	6.34×10^{-3}	NLO	[26]
Single-top (Wt)	MC@NLO 3.3.1 [23]	13.1×10^{-3}	NLO	[26]
WW	HERWIG 6.510 [27]	44.9×10^{-3}	NLO	[26]
WZ ($m_Z > 60$ GeV)	HERWIG 6.510 [27]	18.5×10^{-3}	NLO	[26]
ZZ ($m_Z > 60$ GeV)	HERWIG 6.510 [27]	5.96×10^{-3}	NLO	[26]
Dijet (e channel, $\hat{p}_{\mathrm{T}} > 15$ GeV)	PYTHIA 6.4.21 [20]	1.2×10^{6}	LO	[20]
Dijet (μ channel, $\hat{p}_{\mathrm{T}} > 8$ GeV, $p^{\mu}_{\mathrm{T}} > 8$ GeV)	PYTHIA 6.4.21 [20]	10.6×10^{6}	LO	[20]

Table 2: Background simulated event samples used in this analysis, including the production cross section (multiplied by the relevant branching ratio, BR). The variable $\hat{p}_{\mathrm{T}}$ is the average p_{T} of the two outgoing partons involved in the hard-scattering process, evaluated before modifications from initial- and final-state radiation and from the underlying event. The $t\bar{t}$ cross section is given at next-to-leading-order (plus next-to-next-to-leading-log, NNLL), and the dijet cross sections are given at leading-order (LO) in pQCD. The Z+jets samples were normalised using the inclusive cross sections. Details of PDF sets, final-state photon radiation, and underlying event tunes are given in the text.

the luminosity is estimated to be 3.4% [28]. Criteria for electron and muon identification, as well as for event selection, followed closely those of the previous the 1.3 pb^{-1} W+jets cross section analysis [1].

In the electron channel, events were selected online using a trigger that required the presence of at least one electromagnetic cluster in the calorimeter with transverse energy above 15 GeV in the region of $|\eta| < 2.5$. The impact of the trigger efficiency was small for electrons with $E_{\mathrm{T}} > 20$ GeV. In the offline analysis, electrons were required to pass the standard "tight" electron selection criteria [29] with $E_{\mathrm{T}} > 20$ GeV and $|\eta| < 2.47$; electrons in the transition region between the barrel and endcap calorimeter ($1.37 < |\eta| < 1.52$) were rejected. Events were also rejected if there was a second electron passing the "medium" electron selection criteria [29] and the same kinematic selections as above. To reject events from non-isolated electrons such as those from semileptonic heavy flavour decays in multijet events, a calorimeter based isolation requirement was applied. The transverse energy deposited in the calorimeter in a cone of radius $R = 0.2$ around the electron, corrected for any contribution from the electron energy, was required to be less than 4 GeV. This isolation requirement is greater than 96% efficient over all jet multiplicities for prompt electrons originating from decays of W-bosons and reduces the non-isolated electron background by a factor of two. All other electron selection criteria were the same as in Ref. [1].

In the muon channel, events were selected online using a trigger that required the presence of a muon candidate reconstructed in the muon spectrometer consistent with having originated from the interaction region. The candidate was required to have $p_{\mathrm{T}} > 10$ GeV or $p_{\mathrm{T}} > 13$ GeV (depending on the data period) and $|\eta| < 2.4$. Offline, the muons were required to be identified in both ID and MS subsystems and to have $p_{\mathrm{T}} > 20$ GeV and $|\eta| < 2.4$. The same muon selection criteria were applied as in Ref. [1] with the exception of the ID track requirements and the muon isolation. Minor changes to the ID track requirements were made, so as to be consistent with Ref. [30]. The ID-based muon isolation was changed from an absolute isolation of $\Sigma p^{\mathrm{ID}}_{\mathrm{T}} < 1.8$ GeV to a relative isolation of $\Sigma p^{\mathrm{ID}}_{\mathrm{T}}/p^{\mathrm{muon}}_{\mathrm{T}} < 0.1$, using a cone size of $\Delta R < 0.2$. Events were rejected if there was a second muon passing the same kinematic selections and isolation requirements as above.

The calculation of missing transverse energy ($E_{\mathrm{T}}^{\mathrm{miss}}$) and transverse mass ($M_{\mathrm{T}}$) followed the prescription in Refs. [1] and [29]. M_{T} was defined by the lepton and neutrino p_{T} and direction as $M_{\mathrm{T}} = \sqrt{2p_{\mathrm{T}}^{\ell}p_{\mathrm{T}}^{\nu}(1-\cos(\phi^{\ell}-\phi^{\nu}))}$, where the (x, y) components of the neutrino momentum were inferred from the corresponding $E_{\mathrm{T}}^{\mathrm{miss}}$ components. $E_{\mathrm{T}}^{\mathrm{miss}}$ was calculated from the energy deposits in calorimeter cells inside three-dimensional clusters [31]. These clusters were then corrected to take into account the different response to hadrons compared to electrons or photons, as well as dead material and out-of-cluster energy losses [32]. Only clusters within $|\eta| < 4.5$ were used. In the muon channel, $E_{\mathrm{T}}^{\mathrm{miss}}$ was corrected for the muon momentum. Events were required to have $E_{\mathrm{T}}^{\mathrm{miss}} > 25$ GeV and $M_{\mathrm{T}} > 40$ GeV.

After requiring ≥ 1 primary vertex with ≥ 3 associated tracks in the event, the primary vertex was required to be within 200 mm along the beam direction relative to the centre of the detector. In events with multiple vertices along the beam axis, the vertex with the largest Σp_{T}^2 of associated tracks was taken as the primary vertex.

Jets were reconstructed using the anti-k_{t} algorithm [33] with a radius parameter $R = 0.4$ [34, 35]. The efficiency for reconstructing jets was found to be approximately 98% in simulation for jet p_{T} of 20 GeV, rising to close to 100% efficiency for p_{T}=30 GeV jets. Jets arising from detector noise or cosmic rays were rejected [36]. To take into account the differences in calorimeter response to electrons and hadrons and to correct for experimental effects, a p_{T}- and η-dependent factor, derived from simulated events, was applied to each jet to provide an average energy scale correction [34, 35]. Jets were required to have a rapidity of $|y| < 2.8$ and $p_{\mathrm{T}} > 20$ GeV. All jets within $\Delta R < 0.5$ of an electron or muon (that passed the lepton identification requirements) were removed, regardless of the jet p_{T} or rapidity. As in Ref. [1], jets from pile-up interactions were removed by a cut on the jet-vertex fraction (JVF) which was computed for each jet in the event. After associating tracks to jets with a simple matching in ΔR(track, jet), requiring $\Delta R < 0.4$, the JVF was computed for each jet as the scalar sum p_{T} of all matched tracks from the primary vertex divided by the total jet-matched track p_{T} from all vertices. Jets which fell outside of the fiducial tracking region ($|\eta| < 2.5$) or which had no matching tracks were not considered for the JVF cut. Jets for which JVF < 0.75 were rejected.

5 Background Estimates

The major background processes in the electron channel are QCD and leptonic backgrounds. The latter consist of $W \to \tau\nu$ where the tau decays to an electron, $Z \to ee$ where one electron is not identified and hadronic energy in the event is mismeasured, $Z \to \tau\tau$ events, leptonic $t\bar{t}$ decays ($t\bar{t} \to b\bar{b}qq'e\nu$), single-top events and diboson (WW, WZ, ZZ) processes. The QCD background in the electron channel has two components, one where a light flavor jet passes the electron selection and additional energy mismeasurement in the event results in large $E_{\mathrm{T}}^{\mathrm{miss}}$, and the other where a bottom- or charm-hadron decays to an electron. For the muon channel, the main backgrounds arise from semileptonic heavy flavour decays in multijet events and from the leptonic backgrounds from the following sources: $W \to \tau\nu$ where the tau decays to a muon, $Z \to \mu\mu$ where one muon is not identified, $Z \to \tau\tau$, leptonic $t\bar{t}$ and single-top events in the muon channel and diboson processes.

The number of leptonic background events surviving the above selection cuts was estimated with simulated event samples: ALPGEN for vector boson samples (PYTHIA was used for $W \to \tau\nu$ + jets and $Z \to \tau\tau$), POWHEG for $t\bar{t}$ background, MC@NLO for single-top backgrounds and HERWIG for the diboson backgrounds. The simulated leptonic background samples were normalised to the integrated luminosity of the data using the predicted NNLO, NLO+NNLL or NLO cross sections. The number of QCD background events was estimated by fitting, in each jet multiplicity bin, the $E_{\mathrm{T}}^{\mathrm{miss}}$ distribution in the data (without the $E_{\mathrm{T}}^{\mathrm{miss}}$ cut) to a sum of two templates: one for the QCD background and another which included signal and the leptonic backgrounds. In both muon and electron channels, the shapes for the

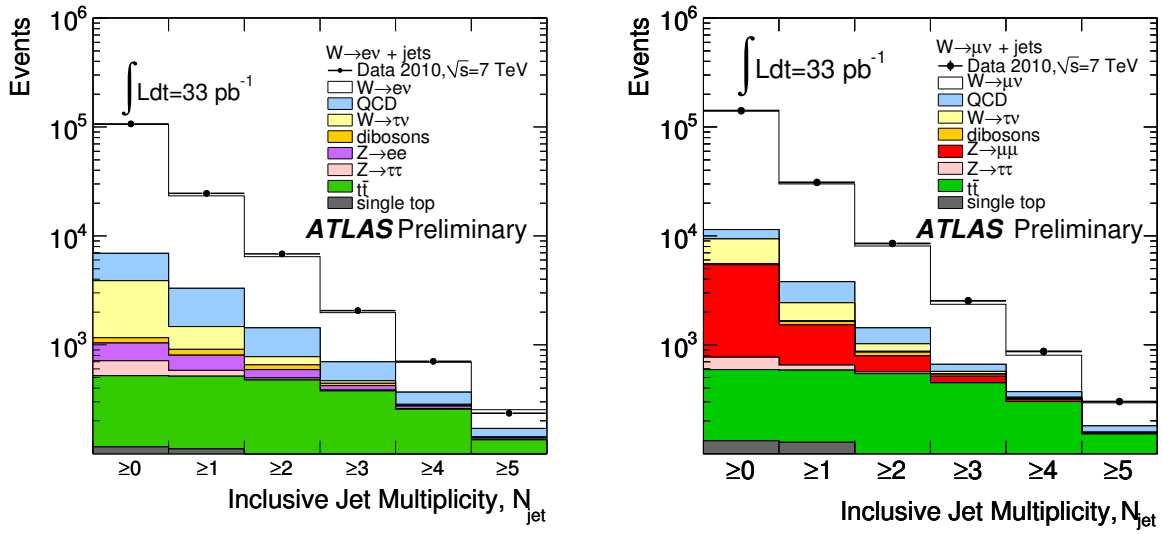

Figure 1: The uncorrected inclusive jet multiplicity distribution. Left: electron channel. Right: muon channel. The signal and leptonic backgrounds are shown using simulations, whereas the QCD background uses the method described in the text. The signal and leptonic backgrounds are normalised to the predicted cross sections.

second template were obtained from simulation. In the muon channel, the QCD template was obtained from simulation. In the electron channel, the template for the QCD background was obtained from the data because the mechanisms by which a jet fakes an electron are difficult to simulate. This template was derived from a data sample where the "loose" electron identification criteria [29] were applied on the shower shapes. The track-cluster matching requirements applied in the standard "tight" electron selection were still applied but the remaining "tight" requirements with respect to the "medium" requirements were required to fail. This ensures that the template for the QCD background is independent from the signal sample. The fit to the $E_{\mathrm{T}}^{\mathrm{miss}}$ distribution was used only to determine the QCD background normalisation, taking into account contributions from leptonic background and signal in the low $E_{\mathrm{T}}^{\mathrm{miss}}$ region. The uncorrected inclusive jet multiplicities for data including the signal and background estimates are shown in Figure 1 for both the electron and muon channels. The W+jets signal yield for the cross section calculation was derived as the difference between the observed number of events after the selection and the sum of background components.

6 Signal Yield

The yield of signal events was corrected back to the particle level, taking into account detector acceptance and reconstruction efficiency. The dominant correction of about 20% in the electron channel comes from electron reconstruction efficiency. In the muon channel, the dominant corrections come from trigger and reconstruction efficiency (corrections of about 10 – 20% and 10%, respectively). The corrections were computed using the ALPGEN W+jets event generator plus full detector simulation, restricting the events to the same phase space as the data analysis. The phase space requirements were applied to generated quantities. In this analysis, particle level jets were constructed in simulated events by applying the jet finder to all final state particles (excluding muons and neutrinos) with a lifetime longer than 10 ps, whether produced directly in the pp collision or from the decay of particles with shorter lifetimes. Correction factors were computed as one-dimensional functions of jet multiplicity, H_{T} and p_{T} of the jets, and were treated as independent. Migration of events across bins of jet p_{T} was made small compared

to the statistical uncertainty by selecting the bin widths to be at least a factor of two larger than the jet p_{T} resolution [34]. Tests with simulated data showed that these correction factors were sufficient to recover particle level distributions. To treat the effect of final state QED radiation, the energy of the generated lepton was defined as the energy of the lepton after radiation plus the energy of all radiated photons within $\Delta R = 0.1$ around the lepton. The systematic uncertainties on the unfolding was estimated by using SHERPA instead of the ALPGEN simulation.

Several scale factors were applied to the data to account for known discrepancies between the data and the simulation. The trigger efficiency in both the muon and electron channel was measured with a sample of $Z \to \ell\ell$ decays. The electron trigger efficiency in data was found to be $99.3 \pm 0.5\%$. For the muon triggers, a trigger efficiency was estimated as a function of muon η and p_{T}. The average muon trigger efficiencies in the barrel (endcap) were 77.3 ± 0.7 (93.6 ± 0.6)%. In both the electron and muon channels, the trigger efficiency (and its uncertainty) from the data was used to correct the simulation. Scale factors, to correct for differences between data and simulation in the electron identification efficiency, were obtained using $W \to e\nu$ and $Z \to ee$ events. The derived scale factors were applied to the simulation as a function of η and ranged from 1% to 8%. The muon reconstruction efficiency scale factors were obtained using $Z \to \mu\mu$ events and were applied as a function of muon η with an average value of 2%.

7 Systematic Uncertainties

The dominant sources of systematic uncertainties in the cross section measurements for both electron and muon channels are the uncertainties in the jet energy scale [34, 35], uncertainties due to pile-up and uncertainties in the lepton reconstruction efficiency. For $N_{\mathrm{jet}} \geq 4$, $t\bar{t}$ cross section uncertainties also become significant. The luminosity uncertainty enters primarily through the signal normalisation but also has an effect on the estimation of the leptonic backgrounds.

Uncertainties in the jet energy scale (JES) and jet energy resolution (JER) were determined from data and simulation [35]. The JES uncertainty varies as a function of jet p_{T} and η, and ranges from around 9% at 20 GeV to about 4.5% above 60 GeV. The JER uncertainty is 10% of the jet energy resolution. To take into account the differences in calorimeter response to quark- and gluon-initiated jets, the uncertainty on the quark-gluon flavor composition [37] was estimated by comparing MC@NLO W+jets simulation to ALPGEN simulation. For jets where a second jet within $\Delta R < 0.6$ is present, an additional 5% uncertainty is added to the JES uncertainty. To estimate the impact of the JES uncertainty, jet energies in the simulated events were coherently shifted by the JES uncertainty, and the $E_{\mathrm{T}}^{\mathrm{miss}}$ vector was recomputed. In addition, energy clusters in the calorimeters not associated to a jet or electron, such as those coming from the underlying event, were scaled using a p_{T}-dependent uncertainty [29], ranging from ±20% for $p_{\mathrm{T}} \simeq 500$ MeV to ±5% at high p_{T}. Similarly the jet energies were smeared by the JER uncertainty and the $E_{\mathrm{T}}^{\mathrm{miss}}$ vector was recomputed. The full analysis was repeated with these variations, and the cross sections were recomputed; the change in the cross section was taken as the systematic uncertainty. The impact of the JES and $E_{\mathrm{T}}^{\mathrm{miss}}$ uncertainties on the cross section uncertainty ranged from 8% for $N_{\mathrm{jet}} \geq 1$ to 26% for $N_{\mathrm{jet}} \geq 4$.

A source of uncertainty in the electron channel is the potential bias in the sample selection for building the template shape of the QCD background. The size of the effect was determined by varying the individual requirements in the electron identification definition. To account for shape differences in the low $E_{\mathrm{T}}^{\mathrm{miss}}$ region, the fit region for the QCD background was varied by using different fit ranges of 0 to 25 GeV and 35 to 100 GeV. The resulting uncertainty on the $N_{\mathrm{jet}} \geq 1$ cross section was 2% dominated by uncertainties in the template shape.

The uncertainties on the lepton reconstruction efficiencies are estimated by comparing the efficiency measured with simulated events to that measured in the data with leptons from $Z \to \ell\ell$ decays, following

e channel		
Effect	Range	Cross Section Uncertainty (%)
Jet energy scale and $E_{\mathrm{T}}^{\mathrm{miss}}$	$\approx 7\%$ (dependent on jet η and p_{T})	+9.8,-7.6
Jet energy resolution	10% on each jet	± 3.3
Electron trigger	±0.5%	± 0.5
Electron reconstruction	±1.5%	± 1.6
Electron correction factors	$\pm 3-5\%$ (dependent on electron η)	+3.3,-3.5
Electron energy scale	±3%	+4.7,-5.2
Electron energy resolution	20% on sampling term	±0.1
	100% (400%) on constant term in barrel (endcap)	
Pile–up removal cut	$4-7\%$ in lowest jet p_{T} bin	+6.6
Residual pile-up effects	from simulation	+3.6
QCD background shape	from template variation	± 1.9
Unfolding	ALPGEN vs. SHERPA	±2.0
Luminosity	±3.4%	± 3.5

μ channel		
Effect	Range	Cross Section Uncertainty (%)
Jet energy scale and $E_{\mathrm{T}}^{\mathrm{miss}}$	$\approx 7\%$ (dependent on jet η and p_{T})	+10.3,-7.6
Jet energy resolution	10% on each jet	± 5.7
Muon trigger	±0.7% (±0.6%) in barrel (endcap)	± 0.5
Muon reconstruction	±1.1%	+1.1,-1.2
Muon momentum scale	±0.4%	± 0.7
Muon momentum resolution	±6%	± 0.1
Pile–up removal cut	$4-7\%$ in lowest jet p_{T} bin	+6.6
Residual pile-up effects	from simulation	+2.6
Unfolding	ALPGEN vs. SHERPA	±1.8
Luminosity	±3.4%	+3.5,-3.8

Table 3: Summary of the systematic uncertainties in the cross section. The uncertainties are shown only for $N_{\mathrm{jet}} \geq 1$. The sign convention for the JES and lepton energy scale uncertainties is such that a positive change in the energy scale results in an increase in the jet or lepton energy observed in the data.

a method similar to that described in Ref. [38]. The uncertainty in the electron reconstruction efficiency was 1.5%. The uncertainty in the muon reconstruction efficiency was 1.1%. The resulting uncertainties in the cross section were approximately 2% in both electron and muon channels.

The uncertainties due to pile-up are dominated by uncertainties in the JVF cut, which include the efficiency of the cut and how well it is modeled in the simulation. As a conservative estimate, the percentage of jets in the data removed by the JVF cut is applied as the uncertainty. This results in a 7% uncertainty for jets with $p_{\mathrm{T}}< 30$ GeV with a resulting uncertainty on the cross section of 7% for $N_{\mathrm{jet}} \geq 1$. Additional uncertainties due to pile-up such as mismodeling of $E_{\mathrm{T}}^{\mathrm{miss}}$ were estimated by calculating the correction factors using simulation without pile-up interactions included. The uncertainties due to pile-up are larger in this note than in Ref. [1] since the average number of pile-up events increased significantly over the running period.

Other uncertainties which were considered include the trigger efficiency, jet reconstruction efficiency,

lepton momentum scale and resolution, and biases in the procedure for correcting for detector effects (for example, by comparing correction factors obtained with ALPGEN to those obtained with SHERPA). Their effect on the cross section was found to be smaller than the uncertainties described before. All of these systematic uncertainties (except for the bias in the template shape for the QCD background in the electron channel) were also applied to the estimates of the QCD and leptonic backgrounds in both electron and muon channels. In addition, for the leptonic backgrounds the uncertainty in the NNLO cross sections was taken to be 5% for W/Z production as in Ref. [29]. The $t\bar{t}$ cross section uncertainty was taken to be approximately 7%, amounting to the sum in quadrature of PDF uncertainties (3%) and uncertainties estimated by varying renormalisation and factorisation scales (6%) [39, 40].

The systematic uncertainties in the cross section measurement are summarised in Table 3 for $N_{\text{jet}} \geq 1$; most of the uncertainties are approximately independent of the jet multiplicity, except for the uncertainty due to the jet energy scale and resolution, and pile-up jet removal.

In the cross section ratio measurement, the uncertainty due to the jet energy scale uncertainty remains the dominant effect, amounting to approximately 5-10% on the ratio. The luminosity uncertainty does not completely cancel in the ratio because the background estimates are affected by the luminosity uncertainty and the background levels vary as a function of jet multiplicity.

8 Next-to-Leading Order pQCD Predictions

The MCFM v5.8 [26] and BLACKHAT-SHERPA [5] predictions were obtained with the same jet algorithm and same kinematic selection requirements as applied to the data. In both cases, renormalisation and factorisation scales were set to $H_{\text{T}}/2$, where H_{T} is the scalar sum of the p_{T} of the unclustered partons and of the lepton and neutrino from the W decay. The PDFs used for MCFM were CTEQ6L1 [11] and CTEQ6.6M [15] for the LO and NLO calculations, respectively. For BLACKHAT-SHERPA CTEQ6.6M was used for both LO and NLO calculations. Corrections for hadronisation and underlying event were computed with PYTHIA as a function of jet multiplicity, jet p_{T} and H_{T}. The effect of final state QED radiation from the electron or muon was computed with ALPGEN and cross checked with PYTHIA and SHERPA, comparing the acceptance before radiation with the acceptance after radiation, but summing up the photons within $\Delta R = 0.1$ around the lepton. This factor ($\simeq 1 - 2\%$) was applied as a correction to the MCFM and BLACKHAT-SHERPA predictions.

The systematic uncertainty in the MCFM and BLACKHAT-SHERPA cross sections due to fragmentation was estimated by comparing PYTHIA W+jets simulation with HERWIG simulation. Underlying event uncertainties were estimated by comparing the AMBT1 [19] event generator tune with the tune from JIMMY [10] as well as by varying the AMBT1 tune to increase the underlying event activity by approximately 10%. Renormalisation and factorisation scale uncertainties were estimated by varying the scales by factors of two, up and down, in all combinations for MCFM and coherently for BLACKHAT-SHERPA. PDF uncertainties were computed by summing in quadrature the dependence on each of the 22 eigenvectors characterising the CTEQ6.6 PDF set; the uncertainty in α_{s} was also taken into account. For MCFM an alternative PDF set, MSTW2008 [13], with its set of 68% C.L. eigenvectors was also examined, and the difference in the central value from CTEQ6.6 and MSTW2008 was taken as the final PDF uncertainty.

9 Results and Conclusions

The measured W+jets cross sections (multiplied by the leptonic branching ratio) and the cross section ratios are shown as a function of the corrected jet multiplicity in Figures 2 and 3. The cross sections are calculated in the limited kinematic region: E_{T}^{j} >20 GeV, $|y^{\text{j}}| < 2.8$, $E_{\text{T}}^{\ell} > 20$ GeV, $|\eta^{\text{e}}| < 2.47$ (excluding

$1.37 < |\eta^{e}| < 1.52$), $|\eta^{\mu}| < 2.4$, $p_{\mathrm{T}}^{\nu} > 25$ GeV, $M_{\mathrm{T}} > 40$ GeV, $\Delta R^{\ell \mathrm{j}} > 0.5$, where ℓ, j and ν denote lepton, jet and neutrino, respectively. The quantities p_{T}^{ℓ}, $|\eta^{\ell}|$, and M_{T} include the energy of all radiated photons within $\Delta R = 0.1$ around the lepton. The W+jets cross section (times leptonic branching ratio) is shown as a function of the p_{T} of the first jet for $N_{\mathrm{jet}} \geq 1$ to $N_{\mathrm{jet}} \geq 4$ events separately in Figure 4, the second jet for $N_{\mathrm{jet}} \geq 2$ to $N_{\mathrm{jet}} \geq 4$ events separately in Figure 5, the third jet for $N_{\mathrm{jet}} \geq 3$ and $N_{\mathrm{jet}} \geq 4$ events separately in Figure 6, the fourth jet for $N_{\mathrm{jet}} \geq 4$ events in Figure 7. The jets are ordered from the highest to lowest p_{T}. Lastly the differential cross section as a function of H_{T} is shown for $N_{\mathrm{jet}} \geq 1$ to $N_{\mathrm{jet}} \geq 4$ in Figure 8. H_{T} is often used as a choice for the renormalisation and factorisation scale and therefore is an interesting comparison between data and predictions.

Also shown in the figures are particle level expectations from ALPGEN and SHERPA simulations as well as a calculation using MCFM. PYTHIA is only shown for the cross section and cross section ratio results as a function of corrected jet multiplicity. As PYTHIA is a LO calculation, it does not provide a good description of the data for jet multiplicities greater than one. The ALPGEN and SHERPA predictions have been normalised to the NNLO inclusive W production cross section. The version of MCFM used here provides NLO predictions at parton level for W boson production with $N_{\mathrm{jet}} \leq 2$; only leading-order predictions are available for W + three jets. The version of BLACKHAT-SHERPA used here provides NLO predictions at parton level for W boson production with $N_{\mathrm{jet}} \leq 3$ and only leading-order predictions for $N_{\mathrm{jet}} = 4$. No additional normalisation was applied to the MCFM and BLACKHAT-SHERPA predictions.

In conclusion, this note presents a measurement of the W+jets cross section as a function of jet multiplicity in pp collisions at $\sqrt{s} = 7$ TeV in both electron and muon decay modes of the W boson, based on an integrated luminosity of 33 pb^{-1} recorded with the ATLAS detector. Measurements are also presented of the ratio of cross sections $\sigma(W+ \geq N_{\mathrm{jet}})/\sigma(W+ \geq N_{\mathrm{jet}} - 1)$ for inclusive jet multiplicities $N_{\mathrm{jet}} = 1 - 5$, of the p_{T} distribution of the first through fourth jets in the event, and of the H_{T} distribution for $N_{\mathrm{jet}} \geq 1$ to $N_{\mathrm{jet}} \geq 4$. The results have been corrected for all known detector effects and are quoted in a limited and well-defined range of jet and lepton kinematics. This range is fully covered by the detector acceptance, so as to avoid model-dependent extrapolations and to facilitate the comparison with theoretical predictions. Good agreement is observed with the predictions of the multi-parton matrix element generators ALPGEN and SHERPA. Calculations based on NLO matrix elements in MCFM (available for jet multiplicities $N_{\mathrm{jet}} \leq 2$) and in BLACKHAT-SHERPA (available for jet multiplicities $N_{\mathrm{jet}} \leq 3$) are also in good agreement with the data.

References

[1] ATLAS Collaboration, *Measurement of the production cross section for W-bosons in association with jets in pp collisions at* $\sqrt{s} = 7$ *TeV with the ATLAS detector*, arXiv:1012.5382 [hep-ex] (2010) accepted by PLB.

[2] CDF Collaboration, *Measurement of the cross section for W-boson production in association with jets in* $p\overline{p}$ *collisions at* $\sqrt{s} = 1.96$ *TeV*, Phys. Rev. **D77** (2008) 011108.

[3] CMS Collaboration, *Rates of Jets Produced in Association with W and Z Bosons in pp collisions at* $\sqrt{s} = 7$ *TeV*, CMS-PAS-EWK-10-012 (2011) .

[4] R. K. Ellis et al., $W + 3$ *jet production at the Tevatron*, Phys. Rev. D **80** (2009) 094002.

[5] C. F. Berger et al., *Precise predictions for* $W + 4$ *jet production at the Large Hadron Collider*, arXiv:1009.2338 [hep-ph] (2010) .

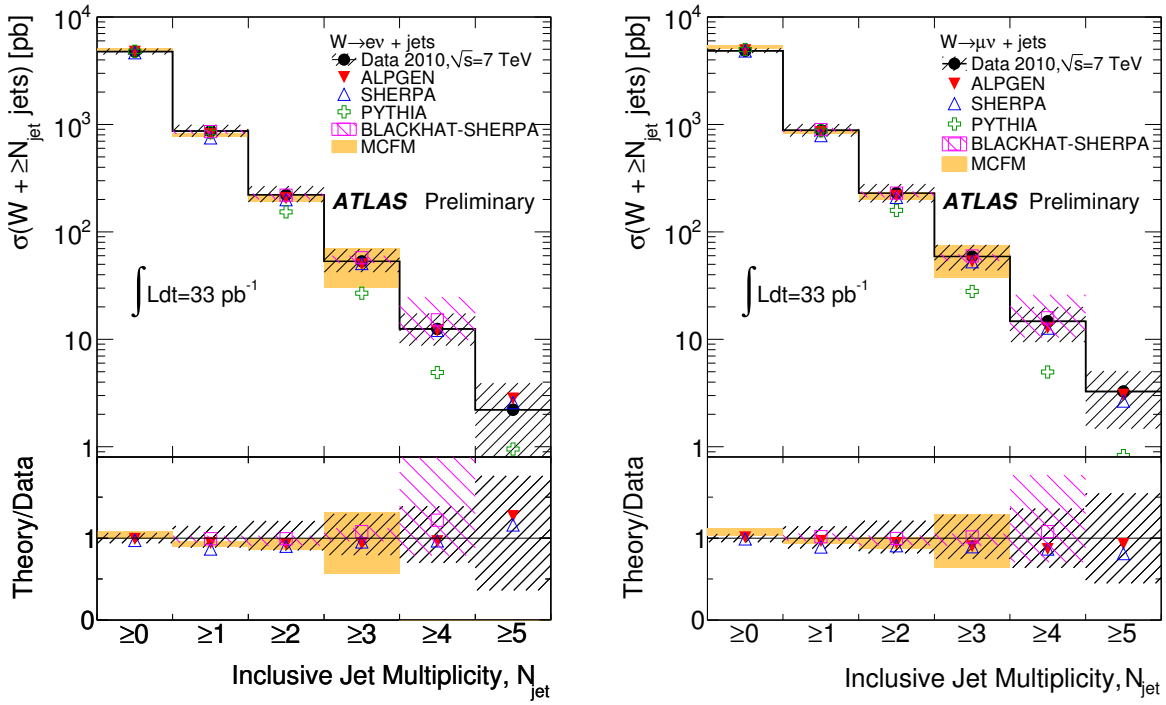

Figure 2: W+jets cross section results as a function of corrected jet multiplicity. Left: electron channel. Right: muon channel. The cross sections are quoted in a limited and well-defined kinematic region, described in the text. For the data, the statistical uncertainties are shown by the vertical bars, and the combined statistical and systematic uncertainties are shown by the black-hashed regions. Also shown are predictions from ALPGEN, SHERPA, PYTHIA, MCFM and BLACKHAT-SHERPA, and the ratio of theoretical predictions to data (PYTHIA is not shown in the ratio). The theoretical uncertainties are shown only for MCFM (NLO prediction for $N_{\text{jet}} \leq 2$ and a LO prediction for $N_{\text{jet}} = 3$) and BLACKHAT-SHERPA (NLO prediction for $N_{\text{jet}} \leq 3$ and a LO prediction for $N_{\text{jet}} = 4$).

[6] ATLAS Collaboration, *The ATLAS Experiment at the CERN Large Hadron Collider*, JINST **3** (2008) S08003.

[7] ATLAS Collaboration, *Expected Performance of the ATLAS Experiment - Detector, Trigger and Physics*, arXiv:0901.0512 [hep-ex] (2009) .

[8] ATLAS Collaboration, *The ATLAS Simulation Infrastructure*, Eur. Phys. J. C (2010) 787.

[9] S. Agostinelli et al., *GEANT4 - a simulation toolkit*, Nucl. Inst. and Meth **A506** (2003) 250.

[10] J. M. Butterworth, J. R. Forshaw, and M. H. Seymour, *Multiparton interactions in photoproduction at HERA*, Z. Phys. **C72** (1996) 637.

[11] J. Pumplin et al., *New generation of parton distributions with uncertainties from global QCD analysis*, JHEP **07** (2002) 012.

[12] A. Sherstnev and R. Thorne, *Parton distributions for LO generators*, Eur. Phys. J. **C55** (2008) 553.

[13] A. D. Martin, W. J. Stirling, R. S. Thorne, and G. Watt, *Parton distributions for the LHC*, Eur. Phys. J. **C63** (2009) 189.

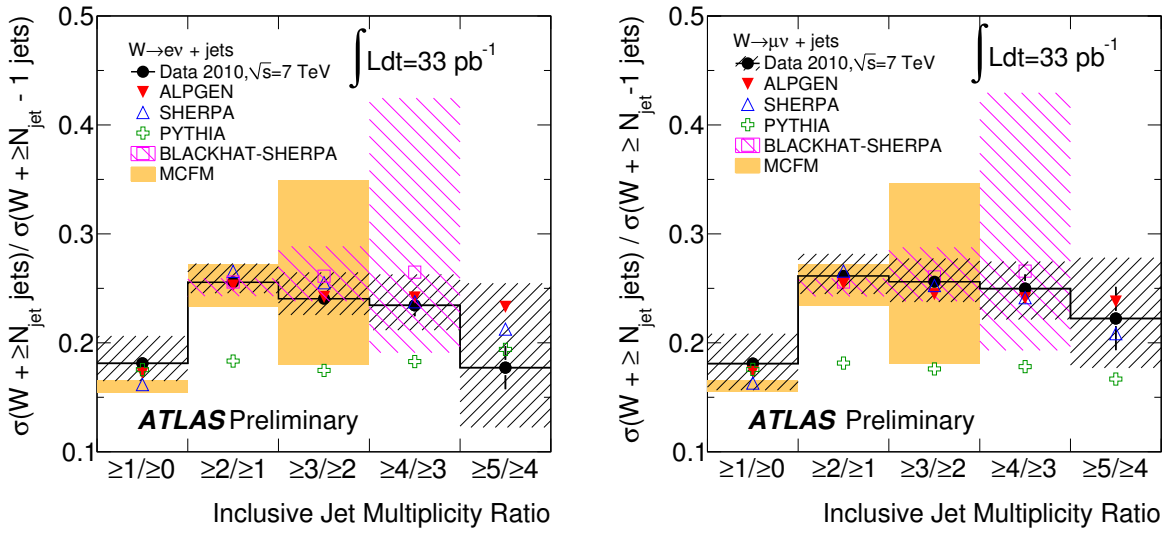

Figure 3: W+jets cross section ratio results as a function of corrected jet multiplicity. Left: electron channel. Right: muon channel. The cross sections are quoted in a limited and well-defined kinematic region, described in the text. For the data, the statistical uncertainties are shown by the vertical bars, and the combined statistical and systematic uncertainties are shown by the black-hashed regions. Also shown are predictions from ALPGEN, SHERPA, PYTHIA, MCFM and BLACKHAT-SHERPA. The theoretical uncertainties are shown only for MCFM (NLO prediction for $N_{\text{jet}} \leq 2$ and a LO prediction for $N_{\text{jet}} = 3$) and BLACKHAT-SHERPA (NLO prediction for $N_{\text{jet}} \leq 3$ and a LO prediction for $N_{\text{jet}} = 4$).

[14] K. Melnikov and F. Petriello, *Electroweak gauge boson production at hadron colliders through* $O(\alpha_s^2)$, Phys. Rev. **D74** (2006) 114017.

[15] P. M. Nadolsky et al., *Implications of CTEQ global analysis for collider observables*, Phys. Rev. **D78** (2008) 013004.

[16] P. Golonka and Z. Was, *PHOTOS Monte Carlo: a precision tool for QED corrections in Z and W decays*, Eur. Phys. J. **C45** (2006) 97.

[17] N. Davidson et al., *Universal interface of TAUOLA technical and physics documentation*, arXiv:1002.0543 [hep-ph] (2010) .

[18] ATLAS Collaboration, *ATLAS Monte Carlo tunes for MC09*, ATLAS-PHYS-PUB-2010-002 (2010) .

[19] ATLAS Collaboration, *Charged particle multiplicities in pp interactions at* $\sqrt{s} = 0.9$ *and 7 TeV in a diffractive limited phase space measured with the ATLAS detector at the LHC and a new PYTHIA6 tune*, ATLAS-CONF-2010-031 (2010) .

[20] T. Sjöstrand, S. Mrenna, and P. Skands, *PYTHIA 6.4 physics and manual*, JHEP **05** (2006) 026.

[21] M. L. Mangano et al., *ALPGEN, a generator for hard multiparton processes in hadronic collisions*, JHEP **0307** (2003) 001.

[22] T. Gleisberg et al., *Event generation with SHERPA 1.1*, JHEP **0902** (2009) 007.

[23] S. Frixione and B. R. Webber, *Matching NLO QCD computations and parton shower simulations*, JHEP **0206** (2002) 029.

[24] S. Frixione, P. Nason, and C. Oleari, *Matching NLO QCD computations with parton shower simulations:the POWHEG method*, JHEP **11** (2007) 070.

[25] R. Bonciani, S. Catani, M. L. Mangano, and P. Nason, *NLL resummation of the heavy-quark hadroproduction cross-section*, Nucl. Phys. **B529** (1998) 424.

[26] J. M. Campbell, R. K. Ellis, and D. L. Rainwater, *Next-to-leading order QCD predictions for W+2jet and Z+2jet production at the CERN LHC*, Phys. Rev. **D68** (2003) 094021.

[27] G. Corcella et al., *HERWIG 6.5: an event generator for Hadron Emission Reactions With Interfering Gluons (including supersymmetric processes)*, JHEP **0101** (2001) 010.

[28] ATLAS Collaboration, *Updated Luminosity Determination in pp collisions at* $\sqrt{s} = 7$ *TeV Using the ATLAS Detector*, ATLAS-CONF-2011-011 (2011) .

[29] ATLAS Collaboration, *Measurement of the* $W \to \ell\nu$ *and* $Z \to \ell\ell$ *production cross-sections in proton-proton collisions at* $\sqrt{s} = 7$ *TeV with the ATLAS detector*, JHEP **12** (2010) 060.

[30] ATLAS Collaboration, *Determination of the muon reconstruction efficiency in ATLAS at the Z resonance in proton-proton collisons at* $\sqrt{s} = 7$ *TeV*, ATLAS-CONF-2011-008 (2011) .

[31] W. Lampl et al., *Calorimeter Clustering Algorithms: Description and Performance*, ATL-LARG-PUB-2008-002 (2008) .

[32] T. Barillari et al., *Local Hadron Calibration*, ATL-LARG-PUB-2009-001 (2009) .

[33] M. Cacciari, G. P. Salam, and G. Soyez, *The anti-*k_t *jet clustering algorithm*, JHEP **04** (2008) 063.

[34] ATLAS Collaboration, *Measurement of inclusive jet and dijet cross sections in proton-proton collisions at 7 TeV centre-of-mass energy with the ATLAS detector*, Eur. Phys. J. C. **71** (2011) 1–59.

[35] ATLAS Collaboration, *Update on the jet energy scale systematic uncertainty for jets produced in proton-proton collisions at* $\sqrt{s} = 7$ *TeV measured with the ATLAS detector*, ATLAS-CONF-2011-007 (2011) .

[36] ATLAS Collaboration, *Data-Quality Requirements and Event Cleaning for Jets and Missing Transverse Energy Reconstruction with the ATLAS Detector in Proton-Proton Collisions at a Center-of-Mass Energy of* $\sqrt{s} = 7$ *TeV*, ATLAS-CONF-2010-038 (2010) .

[37] ATLAS Collaboration, *Light-quark and gluon jets calorimeter response, jet energy scale systematics and sample characterization*, ATLAS-CONF-2011-053 (2011) .

[38] ATLAS Collaboration, *A measurement of the total* $W\pm$ *and* $Z/\gamma*$ *cross sections in the electron and muon decay channels and of their ratios in pp collisions at* $\sqrt{s} = 7$ *TeV with the ATLAS detector*, ATLAS-CONF-2011-041 (2011) .

[39] S. Moch and P. Uwer, *Theoretical status and prospects for top-quark pair production at hadron colliders*, Phys. Rev. **D78** (2008) 034003.

[40] M. Beneke, M. Czakon, P. Falgari, A. Mitov, and C. Schwinn, *Threshold expansion of the* $gg(q\overline{q}) \to Q\overline{Q} + X$ *cross section at* $O(\alpha_s^4)$, Phys. Lett. **B690** (2010) 483.

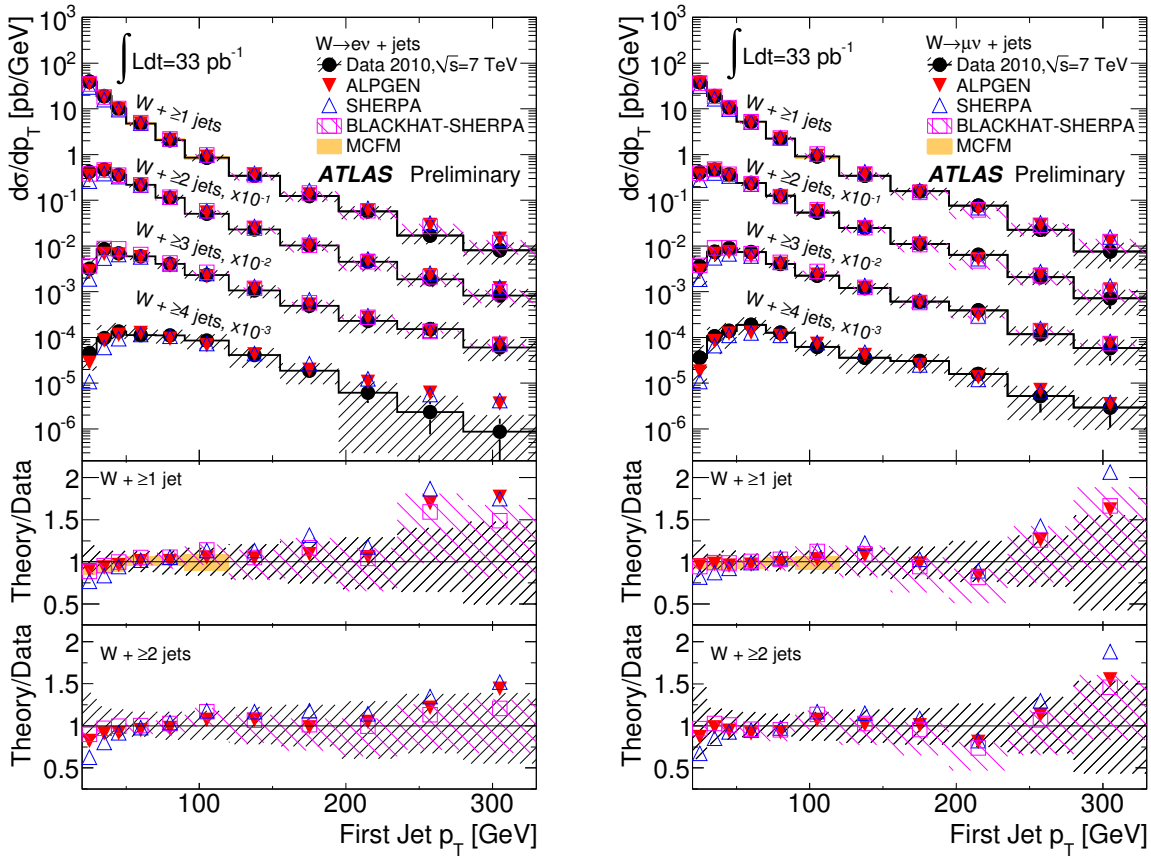

Figure 4: W+jets cross section as a function of the p_{T} of the first jet in the event. The p_{T} of the first jet is shown separately for events with ≥ 1 jet to ≥ 4 jet. The ≥ 2 jet, ≥ 3 jet and ≥ 4 jet distributions have been scaled down by factors of 10 and 100, 1000 respectively. Left: electron channel. Right: muon channel. The cross sections are quoted in a limited and well-defined kinematic region, described in the text. For the data, the statistical uncertainties are shown by the vertical bars, and the combined statistical and systematic uncertainties are shown by the black-hashed regions. Also shown are predictions from ALPGEN, SHERPA, MCFM and BLACKHAT-SHERPA, and the ratio of theoretical predictions to data for ≥ 1 jet to ≥ 2 jet events. The theoretical uncertainties are shown only for MCFM (NLO prediction for $N_{\mathrm{jet}} \leq 2$ and a LO prediction for $N_{\mathrm{jet}} = 3$) and BLACKHAT-SHERPA (NLO prediction for $N_{\mathrm{jet}} \leq 3$ and a LO prediction for $N_{\mathrm{jet}} = 4$).

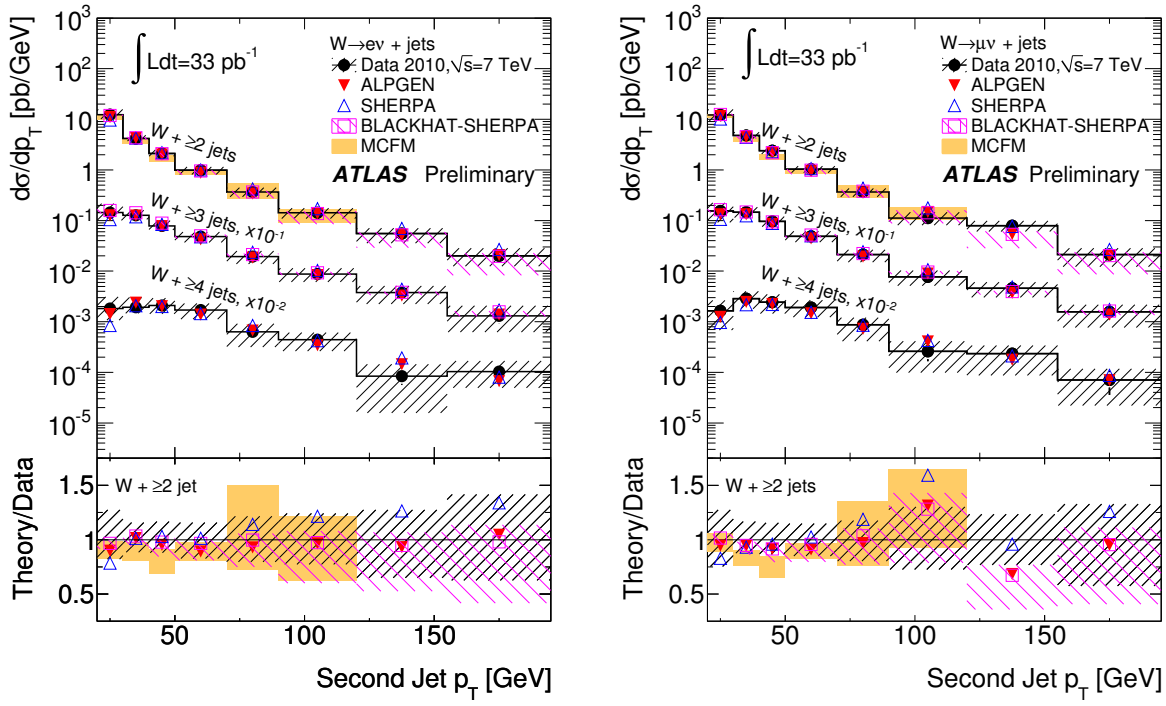

Figure 5: W+jets cross section as a function of the p_{T} of the second jet in the event. The p_{T} of the second jet is shown separately for events with ≥ 2 jet to ≥ 4 jet. The ≥ 3 jet and ≥ 4 jet distributions have been scaled down by factors of 10 and 100 respectively. Left: electron channel. Right: muon channel. The cross sections are quoted in a limited and well-defined kinematic region, described in the text. For the data, the statistical uncertainties are shown by the vertical bars, and the combined statistical and systematic uncertainties are shown by the black-hashed regions. Also shown are predictions from ALPGEN, SHERPA, MCFM and BLACKHAT-SHERPA, and the ratio of theoretical predictions to data for ≥ 2 jet events. The theoretical uncertainties are shown only for MCFM (NLO prediction for $N_{\mathrm{jet}} \leq 2$ and a LO prediction for $N_{\mathrm{jet}} = 3$) and BLACKHAT-SHERPA (NLO prediction for $N_{\mathrm{jet}} \leq 3$ and a LO prediction for $N_{\mathrm{jet}} = 4$).

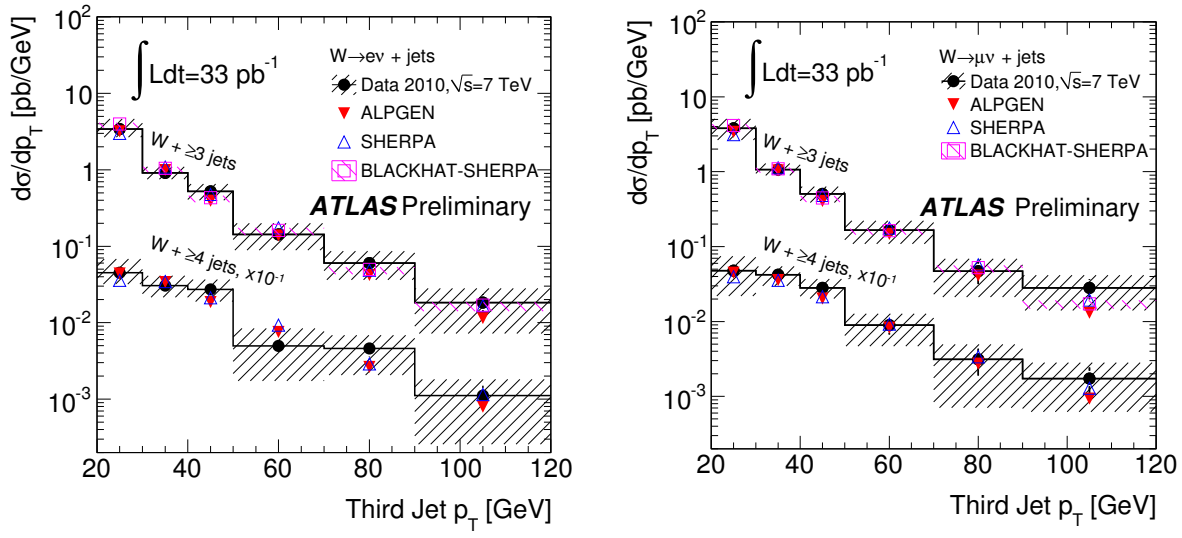

Figure 6: W+jets cross section as a function of the p_{T} of the third jet in the event. The p_{T} of the third jet is shown separately for events with ≥ 3 jet to ≥ 4 jet. The ≥ 4 jet distributions have been scaled down by a factor of 10. Left: electron channel. Right: muon channel. The cross sections are quoted in a limited and well-defined kinematic region, described in the text. For the data, the statistical uncertainties are shown by the vertical bars, and the combined statistical and systematic uncertainties are shown by the black-hashed regions. Also shown are predictions from ALPGEN, SHERPA and BLACKHAT-SHERPA. The theoretical uncertainties are shown only for BLACKHAT-SHERPA (NLO prediction for $N_{\mathrm{jet}} \leq 3$ and a LO prediction for $N_{\mathrm{jet}} = 4$).

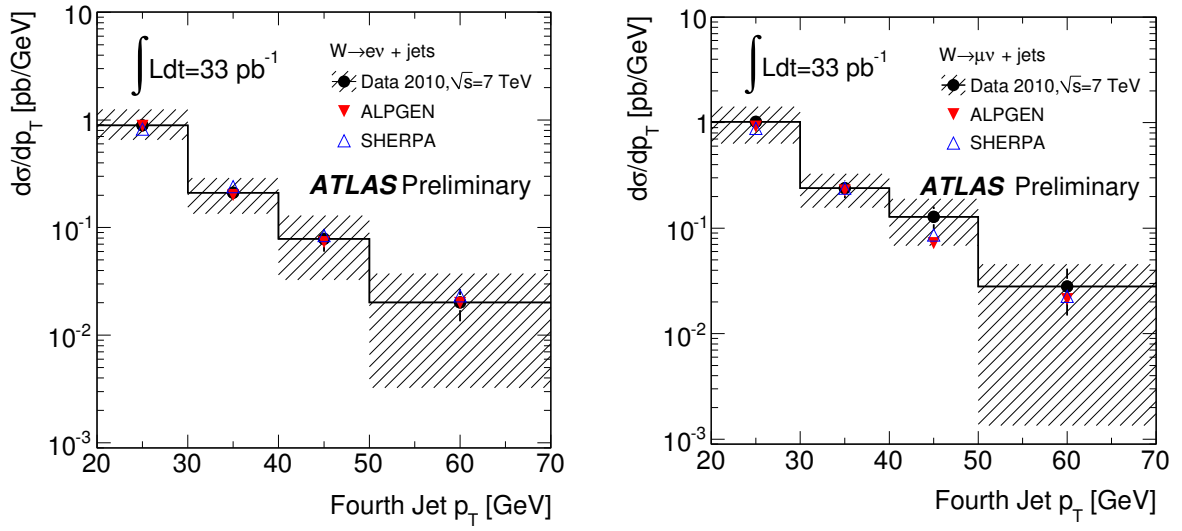

Figure 7: W+jets cross section as a function of the p_{T} of the fourth jet in the event. The p_{T} of the fourth jet is shown for events with ≥ 4 jet. Left: electron channel. Right: muon channel. The cross sections are quoted in a limited and well-defined kinematic region, described in the text. For the data, the statistical uncertainties are shown by the vertical bars, and the combined statistical and systematic uncertainties are shown by the black-hashed regions. Also shown are predictions from ALPGEN, and SHERPA.

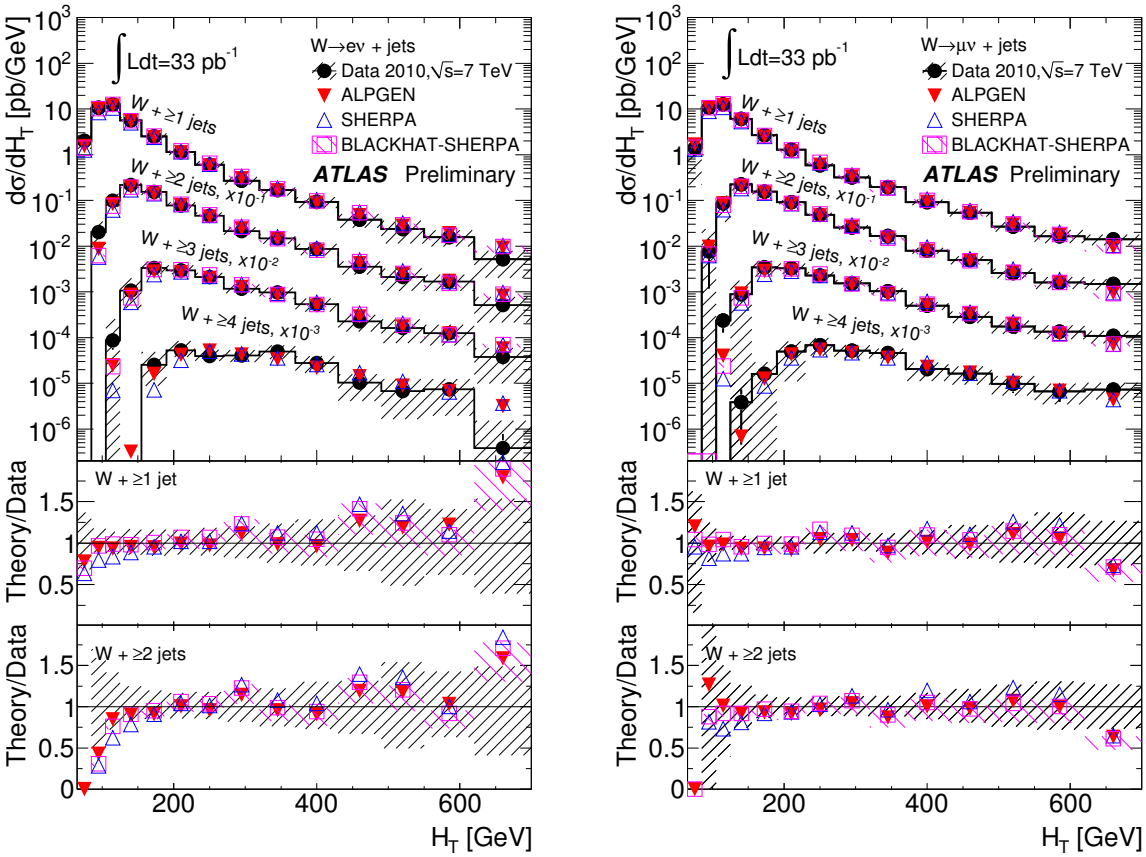

Figure 8: W+jets cross section as a function of H_{T}, shown separately for ≥ 1 jets to ≥ 4 jets. The ≥ 2 jet, ≥ 3 jet and ≥ 4 jet distributions have been scaled down by factors of 10 and 100, 1000 respectively. Left: electron channel. Right: muon channel. The cross sections are quoted in a limited and well-defined kinematic region, described in the text. For the data, the statistical uncertainties are shown by the vertical bars, and the combined statistical and systematic uncertainties are shown by the black-hashed regions. Also shown are predictions from ALPGEN, SHERPA, and BLACKHAT-SHERPA, and the ratio of theoretical predictions to data for ≥ 1 jet to ≥ 2 jet events. The theoretical uncertainties are shown only for BLACKHAT-SHERPA (NLO prediction for $N_{\mathrm{jet}} \leq 3$ and a LO prediction for $N_{\mathrm{jet}} = 4$).